Structural Engineering and Mechanics, *Vol. 53, No. 3 (2015) 393-410*
DOI: http://dx.doi.org/10.12989/sem.2015.53.3.393

Numerical simulations of interactions between solitary waves and elastic seawalls on rubble mound breakwaters

Yun-Feng Lou, Chuan Luo and Xian-Long Jin*

State Key Laboratory of Mechanical System and Vibration, Shanghai Jiaotong University, 800 Dongchuan RD, Shanghai 200240, People's Republic of China

(Received August 23, 2013, Revised May 20, 2014, Accepted June 19, 2014)

Abstract. Two dimensional numerical models and physical models have been developed to study the highly nonlinear interactions between waves and breakwaters, but several of these models consider the effects of the structural dynamic responses and the shape of the breakwater axis on the wave pressures. In this study, a multi-material Arbitrary Lagrangian Eulerian (ALE) method is developed to simulate the nonlinear interactions between nonlinear waves and elastic seawalls on a coastal rubble mound breakwater, and is validated experimentally. In the experiment, a solitary wave is generated and used with a physical breakwater model. The wave impact is validated computationally using a breakwater - flume coupling model that replicates the physical model. The computational results, including those for the wave pressure and the water-on-deck, are in good agreement with the experimental results. A local breakwater model is used to discuss the effects of the structural dynamic response and different design parameters of the breakwater on wave loads, together with pressure distribution up the seawall. A large-scale breakwater model is used to numerically study the large-scale wave impact problem and the horizontal distribution of the wave pressures on the seawalls.

Keywords: wave impact; dynamic response; multi-material ALE; elastic seawalls; breakwater

1. Introduction

Breakwaters are important coastal defense structures for harbor and shore protection. Breakwaters are vulnerable to harsh weather and extremely violent waves. Breakwaters may suffer direct damage from tsunami waves that are triggered by ocean trench earthquakes, such as the Indian Ocean earthquake that was reported in 2004. The interaction between solitary waves and breakwaters has been studied for decades to develop countermeasures to breakwater damage.

The stability of breakwaters in coastal regions has been studied extensively by many researchers using various methods. Cuomo *et al*. (2010) conducted experiments using physical model tests that provided a simple and intuitive set of prediction formulae to calculate quasi-static impact forces and overturning moments. Sakakiyama and Liu (2001) experimentally studied the free surface displacements and velocity field in front of a caisson breakwater with wave-dissipating blocks, where both nonbreaking and breaking waves acted on the caisson breakwater. Hajivalie and

*Corresponding author, Professor , E-mail: jxlong@sjtu.edu.cn

http://www.techno-press.org/?journal=sem&subpage=8 ISSN: 1225-4568 (Print), 1598-6217 (Online)

Yeganeh-Bakhtiary (2011) developed a two-dimensional Reynolds Averaged Navier-Stokes (RANS) model to numerically simulate the shoaling, breaking and overtopping of a solitary wave over a vertical breakwater. A COBRAS-UC model was used to study the overtopping and stability of the breakwater under a wave impact (Losada *et al*. 2008, Guanche *et al*. 2009, Hsiao *et al*. 2010).

In most studies on wave-structure interactions, the structure is assumed to be rigid and elasticity effects are neglected. However, the elasticity of structures should be considered in some situations, such as large floating structures (VLFS) (Zhao and Hu 2012), structures subjected to large wave impacts (e.g., breaking wave impacts on ship hulls and sloshing impacts on tank walls) (Sriram and Ma 2012), etc. 'Hydroelasticity' has been recognized as an important factor in these cases. Thus, both the wave and structural dynamics must be simultaneously accounted for. Alternative methods, such as the particle finite element method (PFEM) (Pin *et al*. 2007) and smoothed particle hydrodynamics (SPH) (Antoci *et al*. 2007), have been well developed for the numerical simulation of the interaction between an incompressible fluid and an elastic structure.

Note that strongly nonlinear and large deformations in a fluid-structure interaction (FSI) creates difficulties in defining the structure and the fluid domain in a unified coordinate system, making it very complicated to study nonlinear FSI and large deformations using Lagrangian or Eulerian descriptions separately. The two media are usually coupled using an Arbitrary-Lagrangian Eulerian (ALE) formulation for the fluid (Tallec and Mouro 2000).

Hirt *et al*. (1997) introduced the ALE method, which has been used in FSI analysis (Nitikitpaiboon and Bathe 1993, Souli *et al*. 2000) and successfully applied to a wide range of problems. Bathe *et al*. (1999) studied the interaction between a fluid and a structure that undergoes a large deformation. The ALE formulation was used to solve for the fluid response for a structural interface and free surface conditions. Pal *et al*. (2003) using a mixed Eulerian-Lagrangian approach to study the free surface oscillation of the liquid in elastic containers. ALE was successfully applied to study the development and dissolution of a non-linear second-order Stokes wave (Zhu *et al*. 2012). The ALE method has only recently been applied to highly nonlinear wave-breakwater interactions simulations: Yang *et al*. (2010) used a weakly compressible ALE method to simulate fluid flow. Although the ALE method has proved to be an effective solution for FSI problems, some researchers have argued that the efficiency of this method may be compromised its intensive computational requirements (Anghileri *et al*. 2005). With the advent of high-performance computers and parallel computing technology (Kalro and Tezduyar 2000, Paik *et al*. 2006), solutions have been generated, and the application of ALE has been promoted.

In the present study, the ALE method is applied to investigate the interaction between a solitary wave and elastic structures. The penalty method is used to address the coupling between waves and structural dynamics. A damping coefficient is used in this method, yielding a relatively smoother time history for the pressure that is shown to be crucial for successfully simulating problems on wave-structure interactions. We exploit this high computational efficiency in a simulation using an explicit integration scheme in LS-DYNA on the Shanghai Supercomputing Center Computing platform. The paper is organized as follows: in Section 2, the ALE method and the penalty method for the FSI are briefly described; in Section 3, the physical model tests are presented, and the numerical models are introduced in Section 4. In Section 5, the results obtained from the numerical simulations are compared with the experimental data to validate the ALE method. The method is then applied to a practical project and analyzed. The principal conclusions of the study are presented in Section 6.

2. Numerical method

2.1 Arbitrary Lagrangian Eulerian approach (ALE)

The ALE description allows for an arbitrary motion of the reference domain, thereby offering an advantage over a material or spatial description. Therefore, a large deformation can be conveniently described together with a moving fluid boundary.

In the ALE formulation, the conservation of momentum and mass for incompressible Newtonian fluids are represented by the Navier–Stokes equations and the continuity equation, as follows

$$\rho \left.\frac{\partial v_i}{\partial t}\right|_{\chi} + \rho c_j \frac{\partial v_i}{\partial \chi_j} = \frac{\partial \sigma_{ij}}{\partial \chi_j} + \rho b_i \tag{1}$$

$$\left.\frac{\partial \rho}{\partial t}\right|_{\chi} + c_i \frac{\partial \rho}{\partial \chi_i} + \rho \frac{\partial v_i}{\partial \chi_i} = 0 \tag{2}$$

where b_i represents the body force. $v_i=v_i(x_i,t)$ is the material velocity field in the space coordinate system x, χ denotes the ALE coordinate system, and ρ is the partial derivative of the density in the ALE coordinate system. The ALE convective velocity $c = v - \bar{v} = \frac{\partial \varphi(X,t)}{\partial t} - \frac{\partial \phi(X,t)}{\partial t} = \frac{\partial x}{\partial \chi} \cdot \frac{\partial \psi^{-1}(X,t)}{\partial t}$ is the difference between the material velocity v and the mesh velocity $\bar{v}$.

The constitutive equation for a Newtonian fluid can be written as

$$\sigma_{ij} = -p\delta_{ij} + \tau_{ij} \tag{3}$$

where the deviatoric stress is given by $\tau_{ij} = \lambda \delta_{ij} s_{kk} + 2\mu s_{ij}$, $s_{ij} = 1/2((\partial v_i / \partial x_j) + (\partial v_j / \partial x_i))$.

The first term on the right-hand side of Eq. (3) is defined by an equation of state (EOS) in the simulation. In this study, we consider a weakly compressible Newtonian fluid for which the viscous stress $\lambda \delta_{ij} s_{kk}$ is approximately zero and is thus neglected. The second term on the right-hand side of Eq. (3) only includes the shear stress $2\mu s_{ij}$. Thus, Eq. (3) can be rewritten as

$$\sigma_{ij} = -p\delta_{ij} + 2\mu s_{ij} \tag{4}$$

where μ is the kinematic viscosity which is a constant value for a Newtonian fluid.

The constitutive equation for the fluid flow is composed of the EOS and the material model. The EOS defines the volumetric compression (or expansion) behavior of the fluid, and the material model defines the relationship between the shear stress and the shear strain rate. The Gruneisen equation and a polynomial equation of state are chosen as the EOSs for water and air, respectively.

2.2 Explicit dynamic analysis

The equation of motion for the nonlinear case at time t_n is given by

$$M\ddot{U}_n + C\dot{U}_n + F_n^{\text{int}}(U_n) = P_n \tag{5}$$

where M is the mass matrix; C is the damping coefficient matrix; P_n accounts for the external and body force vector; F_n^{int} is the internal force vector; and $\ddot{U}_n$, $\dot{U}_n$, and U_n are the acceleration, velocity and displacement vectors, respectively. Eq. (5) can be integrated using an explicit central difference integration rule and is rewritten as follows

$$\ddot{U}_n = M^{-1}\left[P_n - C\dot{U}_n - F_n^{\text{int}}(U_n)\right] \tag{6}$$

The velocities and displacements are updated in each time step as follows

$$\dot{U}_{n+1/2} = \dot{U}_{n-1/2} + \Delta t_n \ddot{U}_n \tag{7}$$

$$U_{n+1} = U_n + \Delta t_{n+1/2}\dot{U}_{n+1/2} \tag{8}$$

where $\Delta t_n=(\Delta t_n+\Delta t_{n+1})/2$

The explicit integration scheme improves the computational efficiency by using a diagonal mass matrix because it is trivial to invert the mass matrix in Eq. (6). One of the disadvantages of this explicit integration procedure is that the stability of the scheme depends on the time step size. For numerical stability, the calculation time step size must be smaller than the critical time step Δt_{cr}, which is determined by the characteristic length of the element and its material properties. For constant strain and rate-independent materials, the critical time step can be calculated using $\Delta t_{ct} \le \min_e (l_e / c_e)$, where l_e is the characteristic length of the element and c_e is the wave speed in the element.

The destabilizing effects of nonlinearities are accounted for by introducing a reduction factor T_s, where $\Delta t_n=T_s\Delta t_{ct}$. This reduction factor should satisfy $0.67\le T_s\le 0.90$. In this study, we choose $T_s=0.80$ to account for the high contact nonlinearities in the wave impaction simulation.

The set of ALE equations is usually solved for using an operator-split procedure. Each time increment from t to $t+\Delta t$ is divided into two successive steps.

The procedure over the first time increment is performed exactly as in the classical Lagrangian case. In the Lagrangian step, the mesh follows the material ($\rho \left.\frac{\partial v_i}{\partial t}\right|_x = \frac{\partial \sigma_{ij}}{\partial x_j} + \rho b_i$) until an equilibrated Lagrangian configuration is obtained.

The second step, which is called an Eulerian step, is divided into two substeps: an appropriate mesh velocity is defined by relocating each node of the mesh to a more suitable position, followed by transferring the data from the old mesh configuration to the new configuration. This new configuration of the nodes is called an Eulerian configuration.

2.3 Fluid structure interaction

In this study, we account for the dynamic response of the structure to the wave impact. Thus, the deformation of the breakwater structure is described by Eq. (9) using a constitutive equation for St. Venant's elastic bodies

$$\rho_s \left.\frac{\partial^2 u}{\partial t^2}\right|_X = \frac{\partial \sigma_{ij}}{\partial x_i} + f_i \tag{9}$$

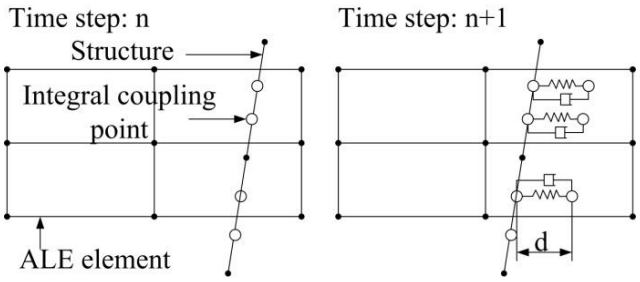

Fig. 1 Wave-structure coupling algorithm

where X denotes the Lagrangian coordinate, ρ_s is the density of the structure, f_i is the body force, and u is the displacement of the structure.

The FSI problems in this study are solved using a penalty-based finite element method in conjunction with ALE. Eqs. (1), (2) and (9) are coupled under the following conditions to obtain geometric compatibility and mechanical equilibrium on the FSI interfaces

$$v_i = v_s = \left.\frac{\partial u}{\partial t}\right|_X \tag{10}$$

$$F_f + F_s = 0 \tag{11}$$

where F_f and F_s are the interaction forces acting on the FSI interfaces.

In this study, the penalty method is chosen to calculate the interaction forces because it is known to be the simplest and most efficient method for solving this problem. Moreover, the penalty method guarantees energy conservation.

The penalty-based coupling system is shown in Fig. 1. The underlying concept of the penalty method is to track the relative displacements between the corresponding coupling nodes on the structure surface and inside the ALE fluid elements. In the penalty method, a coupling force is introduced between the fluid and the structure. The coupling force is defined to be proportional to the penetration depth and the contact rigidity.

To reduce numerical oscillations, a viscous damper system is included to damp out high frequencies. The coupling force can be calculated using the Eq. (12)

$$F_s = \frac{d^2 Z}{dt^2} + \xi \frac{dZ}{dt} + \omega^2 Z \tag{12}$$

where ξ is the damping coefficient; $\omega = \sqrt{k(m_s + m_f)/(m_s - m_f)}$; k is the contact rigidity; and Z represents the penetration for which an iterative solution is obtained using the following equation

$$Z_{n+1} = Z_n + (V^c_{n+1/2} - V^s_{n+1/2}) \cdot \Delta t_{n+1/2} \tag{13}$$

where $V^c_{n+1/2}$ and $V^s_{n+1/2}$ are the velocities of the coupling points in the ALE and the Lagrangian body, respectively.

The primary difficulty associated with this coupling involves the evaluation of the stiffness

coefficient k. In an explicit contact algorithm, this coefficient can be calculated as $k = \alpha K_i A_i^2 / V_i$. Here, K_i is the bulk modulus of the element; A_i is the element area; V_i is the element volume; and α is the scale factor. For numerical stability, the scalar factor should satisfy $0 \leq \alpha \leq 1$. In this study, we choose α=0.5 to ensure the dynamic coupling stability and prevent leakage. At the same time, we adjust the number of coupled integral points and the minimum fluid volume fraction in an ALE element to activate coupling.

3. Physical tests

The experimental studies are conducted on an irregular wave flume at the Zhejiang Institute of Hydraulics and Estuary. The wave flume is 70 m long, 1.2 m wide and 1.2 m deep and is equipped with a push plate-type wave generator at one end. The Froude number $V_M / \sqrt{gL_M}$ and the Strouhal number $V_M T_M / L_M$ are used to scale the physical model to the actual model. Considering the height of the breakwater, the wave characteristics, the water depth, the flume size, etc., a model scaling of 25 is used. A schematic of the experimental breakwater cross section is shown in Fig. 2, and a photograph of the experimental breakwater is shown in Fig. 3. Eight pressure gauges are placed on the seawalls to record the time history of the water impact pressure. The sampling frequency is set to 1000 Hz, and the gauge locations are indicated by circular symbols in Fig. 2. The experiments are recorded by a high-speed video camera to obtain a qualitative understanding of the water-on-breakwater event.

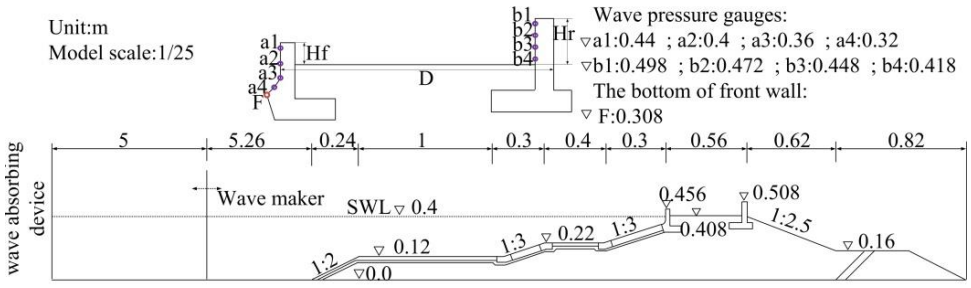

Fig. 2 Schematic of the breakwater cross section

Fig. 3 Photograph of breakwater model used in this study

In the experiment, a push plate wave maker is used for wave generation. The wave maker motion must first be obtained. The theoretical solution for a solitary wave of finite amplitude that propagates without a change in shape is given by

$$\eta = H\,\mathrm{sech}^2[\sqrt{3H/4d^3}\,(x-Ct)]$$

$$C = \sqrt{g(H+d)} \tag{14}$$

The following equations are satisfied at the wave maker surface

$$dS/dt = \bar{u}(x,t)\,, \quad x = S \tag{15}$$

$$\bar{u}(x,t) = C\eta(x,t)/[d+\eta(x,t)] \tag{16}$$

where, S is the displacement of the wave maker, and $\bar{u}(x,t)$ is the average speed in the x-direction.

The equation of the actual wave maker motion can be obtained by integrating Eq. (15)

$$S(t) = \sqrt{\frac{4H}{3d}}\,d\,\tanh[\sqrt{\frac{3H}{4d^3}}(Ct-S)] \tag{17}$$

In the equations above, H is the height of the wave with respect to the unperturbed surface, d is the depth from the bottom to the unperturbed surface, g is the acceleration due to gravity, ρ is the density of water, and η is the elevation of the free surface. This quasi-analytical solution will be compared with the numerical results.

4. Model description

The experimental results are used to develop a three-dimensional simulation model of the breakwater-flume coupling system. The breakwater is constructed using an eight-node hexahedron solid element. The minimum grid spacing of the structure is 5 mm. The friction between the structures is modeled using the Coulomb friction law. The static and dynamic friction coefficients are 0.3 and 0.25, respectively. Table 1 presents the material parameters of the coupling model. In the ALE formulation, the fluid domain (i.e., water and air) is discretized using eight-node hexahedron elements. The ALE elements around the breakwater and the free surface are intensively meshed. The total numbers of nodes and elements are 592,645 and 544272, respectively.

Table 1 Model material parameters

Part	Density (kg/m^3)	Elastic modulus (Pa)	Poisson ratio
Seawall	2.40×10^3	2.00×10^{10}	0.15
Surface protection structure	2.40×10^3	2.00×10^{10}	0.15
Rubble mound	2.00×10^3	5.00×10^{10}	0.30
	Initial destiny	Coefficient of kinematic viscosity	Sound speed in water
Water	1.00×10^3 kg/m^3	8.68×10^{-4}Pa·s	1.48×10^3 m/s

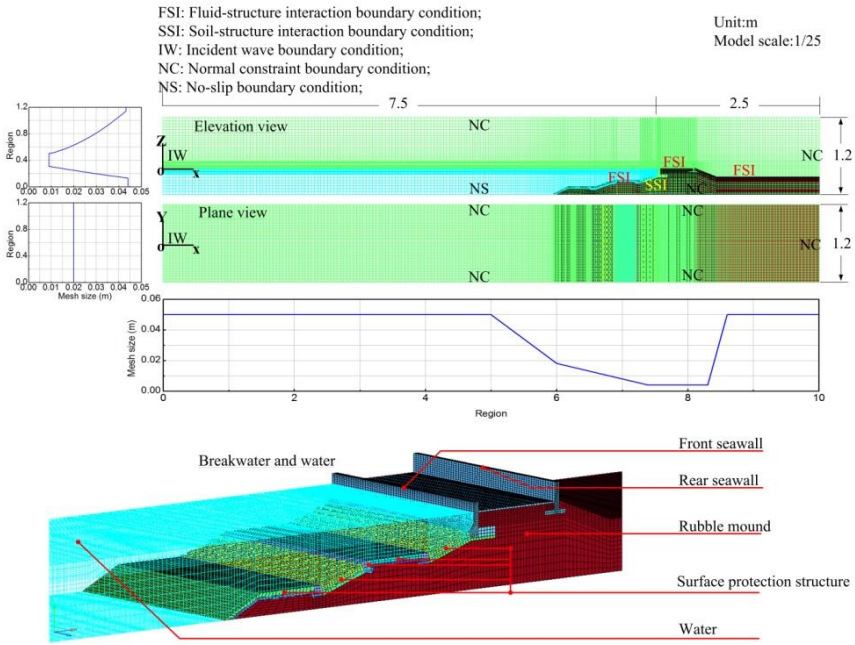

Fig. 4 Experimental model of breakwater - flume coupling system

Table 2 Solution times

Test series	T_s	α	Minimum grid spacing of ALE/Structure[m]	Number of CPUs	Time step [s]	Termination time [s]	Solution CPU time [h]
Experimental Model	0.8	0.5	0.004/0.005	32	1.07e-6	4	93.33
			0.004/0.005	48	1.07e-6	4	76.67
Local Model	0.8	0.5	0.1/0.125	32	3.33e-5	20	24.67
			0.1/0.125	48	3.33e-5	20	20.89
Large-scale Model	0.8	0.5	0.1/0.125	48	3.33e-5	60	108.38

To conserve CPU time, a numerical tank is used that is smaller than the physical wave tank. The resulting 10 m×1.2 m×1.2 m numerical wave flume model is shown in Fig. 4. The boundary conditions are also shown in Fig. 4. Table 2 summarizes the solution times required for various mesh sizes (*de*) and calculation parameters.

The interaction between a solitary wave and a whole coastal breakwater is numerically simulated using a large-scale breakwater. The configuration of the whole coastal breakwater is illustrated in Fig. 5, and the corresponding geometric model is shown in Fig. 6(a). The finite element models for the large-scale breakwater-wave coupling are shown in Figs. 6 (b) and (c). The grid sizes of the breakwater and the ALE of the coupling region in the axial direction are 0.375 m and 0.3 m, respectively. The ratio of the element length to the width does not exceed 4. Other regions in the model are carefully meshed in this study. Most of the elements are brick elements, and the angles of these elements are controlled between 45° and 135°. The number of nodes and elements are 1635994 and 1530024, respectively. The calculation costs approximately 108.38 h with 48 CPUs on a Dawning 5000A supercomputer, as shown in Table 2.

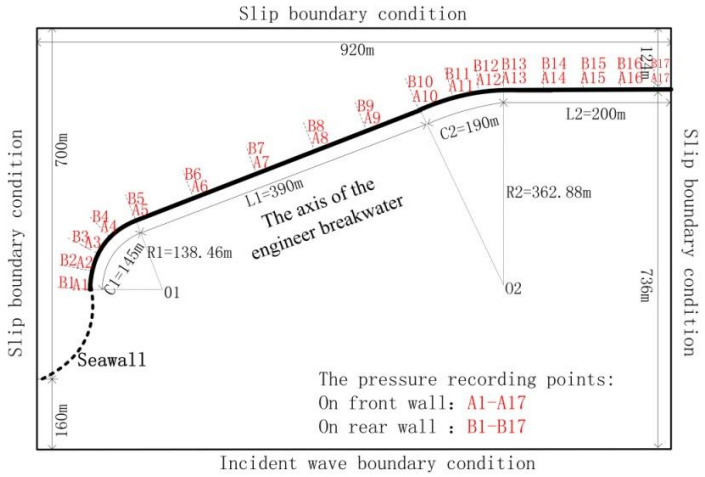

Fig. 5 Scheme of large-scale breakwater - wave coupling model

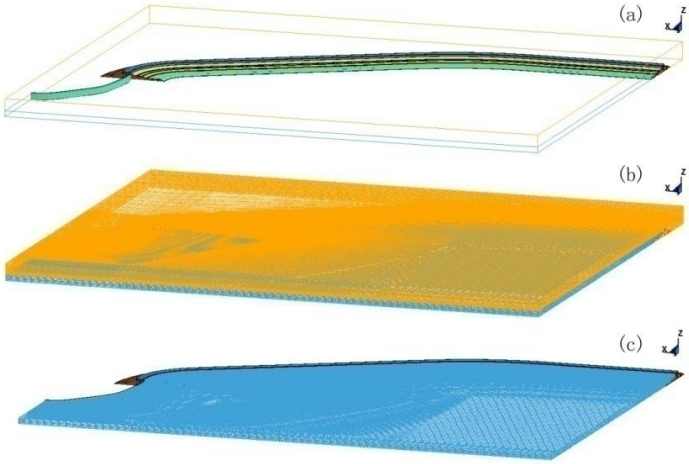

Fig. 6 Large-scale model of breakwater - wave coupling system

5. Results and discussions

The developed simulation model yields the interactions between solitary waves and the breakwater. Herein, we focus on analyzing the breakwater dynamic responses and the wave impact pressure. The numerical results are first compared with the experimental measurements to validate the effectiveness of the simulation model. Then, the ALE method is applied to a practical engineering problem. A local breakwater - wave coupling model, which is proportional to the prototype of the physical model, and a large-scale breakwater - wave coupling model are used for this analysis. The coupling model is used to study the pressure distribution on the wall and the effects of the seawall stiffness and the structural configurations on the wave loads. Table 3 summarizes the different conditions for the applications, which include the water depth H_w, the breakwater width D, the front seawall elevation relative to the breakwater top H_f, the rear seawall elevation relative to the breakwater top H_r, and the wave height H_m.

Table 3 Test conditions

Test series		Configuration	Wave height H_m [m]
Experimental model		H_f=0.048 m, H_r=0.1 m, H_w=0.4 m, D=0.56 m	0.144
Local model	Stiffness discussion	H_f=1.2 m, H_r=2.5 m, H_w=10 m, D=14 m	3.6
	Elevation discussion	H_f=1.2 m; 0.8 m; 0.4 m; 0 m, H_r=2.5 m; 2.75 m; 3.0 m, D=14 m, H_w=10 m	3.6
	Width discussion	H_f=1.2 m, H_r=2.5 m, D=10 m; 14 m; 18 m, H_w=10 m	3.6
Large-scale model		H_f=1.2 m, H_r=2.5 m, H_w=10 m, D=14 m	3.6

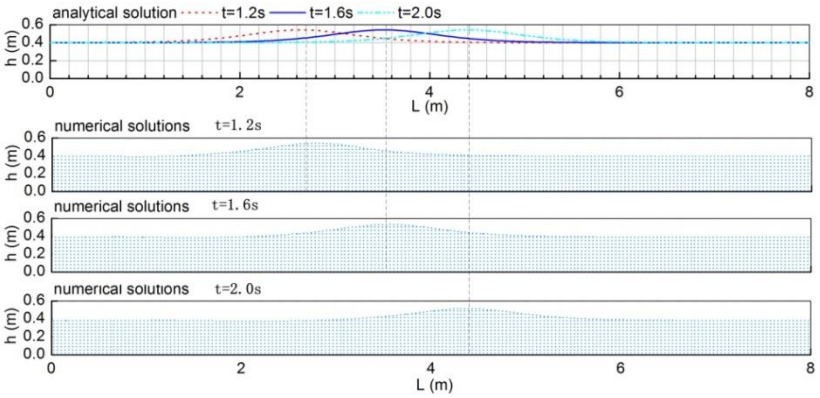

Fig. 7 Comparison between numerical and analytical solutions for solitary wave propagation

5.1 Method validation

In this section, the numerical simulation is validated by comparing the numerical results with those from the analytical solution and the physical tests under the same wave conditions (i.e., H_m=0.144 m and H_w=0.4 m). This wave condition is chosen to simulate the response of the breakwater when subjected to extreme waves under realistic conditions.

In the following section, the results for the wave free surface elevation, the wave evolutionary courses, and the impact pressure acting on the pressure gauges which faces the incoming waves are presented and discussed.

Before the breakwater simulations are conducted, simulations are performed without the structure to compare the undisturbed wave elevation with the theoretical solution. The wave profiles at the same time instant are compared in Fig. 7. The simulation results are in good agreement with the analytical solutions for the range of values over which the analytical solutions are valid. The compared simulation results include the height and shape of the wave.

Fig. 8 shows spatial snapshots of the waves during the evolutionary courses. It includes four wave evolutionary stages: a wave on a sloping beach; water impacting the front wall; water impacting the rear wall and the overtopping of the breakwater. The images obtained from the laboratory experiments and the numerical results are also plotted on the figure for comparison. The

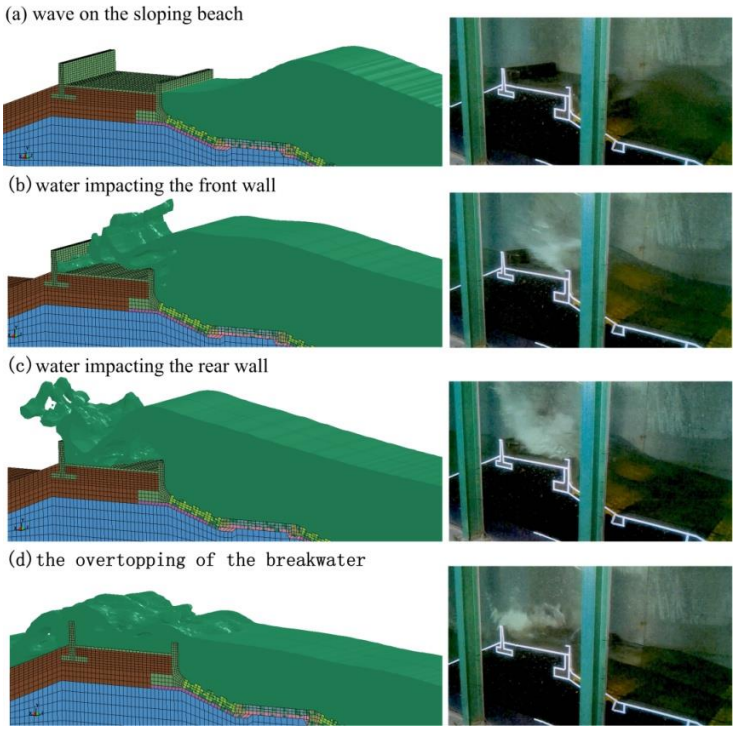

Fig. 8 Qualitative comparison of wave evolution between simulation data (left column) and laboratory images (right column)

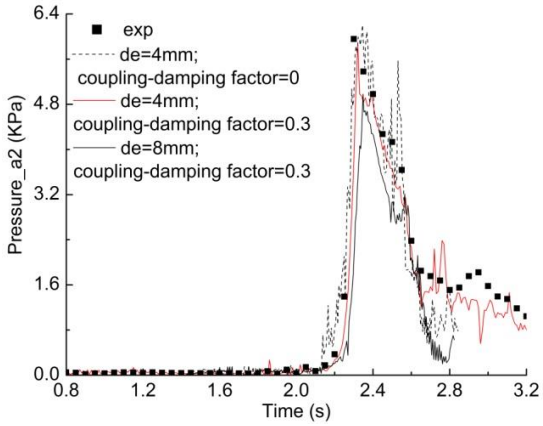

Fig. 9 Comparison of impact pressure for different mesh sizes and coupling coefficients

figures show that the wave approaching the breakwater does not break. The front vertical seawall deflects the wave upward, and the wave evolves into an overtopping flow. Then, the upper fluids directly cross the rear wall. This motion generates a transient splash-up for the reflected jet that is not fully developed. Finally, the fluid violently impacts the rear wall, and then the overtopping of the breakwater. Despite this extremely violent phenomenon, the simulation results are in good agreement with the experiment results.

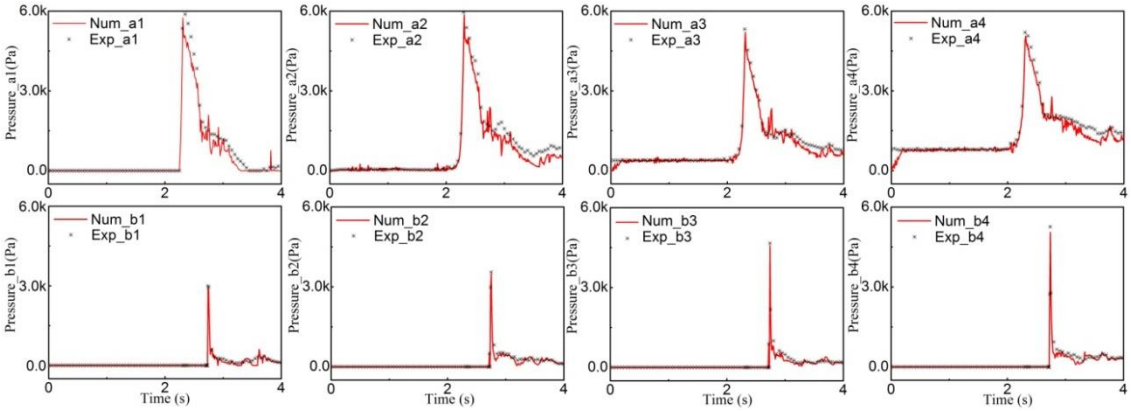

Fig. 10 Comparison between numerical results and experimental results for time history of impact pressure along windward seawall surface

Fig. 9 shows the impact pressure at point a2 for various mesh sizes (*de*). The figure shows that the pressure time history produced by the present method with coupling-damping factor is quite smooth. The large elements used near the coupling region favorably affect the time step required for the explicit time integration. Nevertheless, these large elements are unsuitable for calculating wave impact pressures. The agreement between the results may be improved by increasing the ALE mesh density near the breakwater. The coupling-damping factor that is introduced in this procedure results in a relatively smooth pressure time history, which is crucial for successfully simulating the wave-structure interaction.

Fig. 10 compares the time histories obtained from the simulations and experiments for the impact pressure along the weatherside seawall surface. The numerical results agree well with the laboratory data. The hydrostatic pressure values at points a3 and a4 are 380 Pa and 785 Pa, respectively. These values are very close to the theoretical results.

5.2 Application to local breakwaters and discussion

5.2.1 Structural response effects

Fig. 11 shows the pressure time history on the seawall at points a2 and b4. The figure also shows the corresponding results for a rigid breakwater with the same size and configuration. The time history indicates that for an elastic seawall, the pressure at b4 reaches a maximum value of approximately 126.25 kN/m^2 at 13.05 s, whereas the impact pressure for a rigid wall is approximately 160.33 kN/m^2 at 13.05 s. Thus, the ratio of the maximum pressure of the rigid plate to that of the elastic plate is approximately 1.27. This phenomenon is observed both in our simulation and with a MLPG_R model, as has been reported by (Sriram and Ma 2012).

To analyze the wave pressure distribution, pressure impulses are non-dimensionalized as $P_{max}/\rho g H_m$, where P_{max} is the maximum wave pressure.

The maximum dimensionless pressure impulses on the front seawall for different elastic modulus values are plotted in Fig. 12(a) (Z_f is the position relative to point F up the front seawall). The graph shows that the pressure impulses on the front seawalls attain their maximum values at the still water level (SWL). As anticipated, the impact load on the wall is inversely proportional to the elasticity of baffle; the impact load of the fluid on the wall increases as the elastic modulus of the baffle

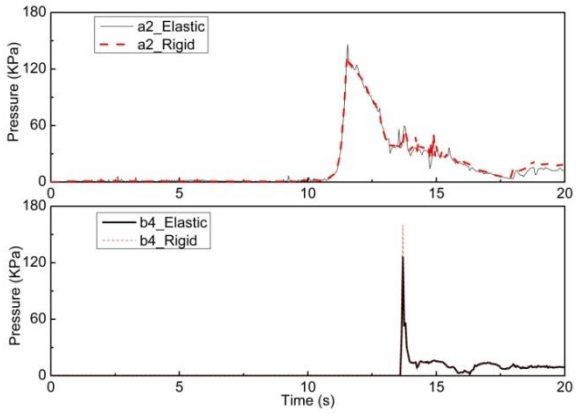

Fig. 11 Pressure time history at a2 and b4

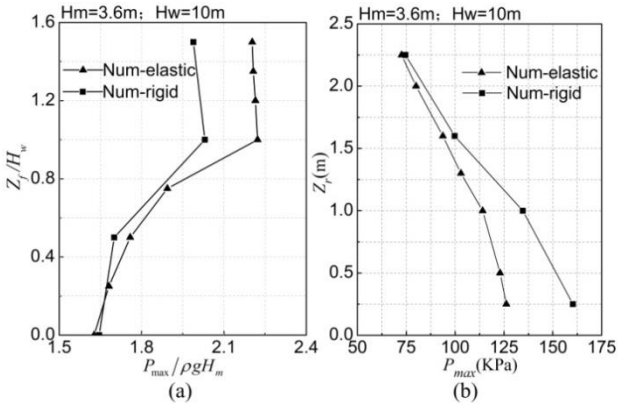

Fig. 12 Comparison between numerical results for pressure impulse distribution up the seawalls

decreases. This result is obtained because a less flexible baffle can absorb a greater amount of fluid momentum (Rafiee and Thiagarajan 2009).

The maximum pressure impulses on the rear seawall for different elastic modulus values are plotted in Fig. 12(b) (Z_r is the position relative to the top of the breakwater up the rear seawall). The graph shows that the structural response weakens the impact pressure on the rear wall relative to the front wall. One possible explanation is that the structural response affects the wave pressure differently for a spill-way impact than for a violent impact.

5.2.2 Seawall elevation effects

In this section, the effect of the seawall elevation on the wave pressure is numerically investigated by varying the elevations of the front and rear seawalls.

The results shown in Figs. 13(a) and (b) include the wave pressure on both the front and rear seawalls, respectively, and the horizontal force on the rear seawall (see Fig. 13(c)). The calculations are performed for the same wave condition with various elevations of the front seawall: H_f=1.2, 0.8, 0.4, and 0. Fig. 13(a) shows the maximum dimensionless pressure impulses on the front seawall. The impact pressures at the SWL increase when the elevation of the front seawall is decreased. In contrast, the impact pressures at the bottom decrease as the elevation of the front seawall decreases.

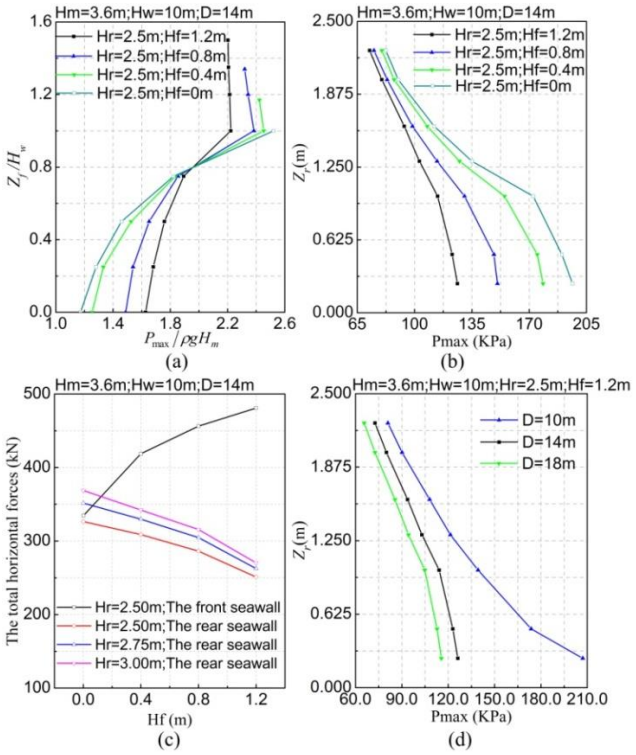

Fig. 13 Pressure impulse and thrust distribution up the front and rear walls

Fig. 13(b) shows the maximum pressure impulses on the rear seawall. The results show that the pressure at the bottom is more sensitive to the change in the elevation of the front wall than the pressure at the top of the rear seawall.

Fig. 13(c) represents the horizontal force on the seawalls for different seawall elevations. In this study, the total horizontal forces (F_h) on the wall are computed as follows

$$F_h = \sum_{k=1}^{4} P_k \cdot \Delta Z \tag{18}$$

where P_k are the numerical pressures at the key points (a1, a2, a3, a4, b1, b2, b3, and b4), and ΔZ is the distance up the wall between two key points

It is obvious that decreasing the elevation of the front seawall decreases the maximum horizontal forces on the front seawall from 480.86 kN to 334.37 kN. However, the maximum horizontal forces on the rear seawall increase from 251.08 kN to 326.41 kN. For the same elevation of the front seawall, the maximum horizontal forces of the rear seawall increase as the elevation of the rear seawall increases from 2.5 m to 3.0 m. In general, the front seawall protects the rear seawall. Additionally, on the premise of the wave overtopping satisfaying the design requirements, the elevation of rear seawall should be as low as possible.

5.2.3 Breakwater width effects

In this section, the effect of the breakwater width on the wave pressure is investigated numerically.

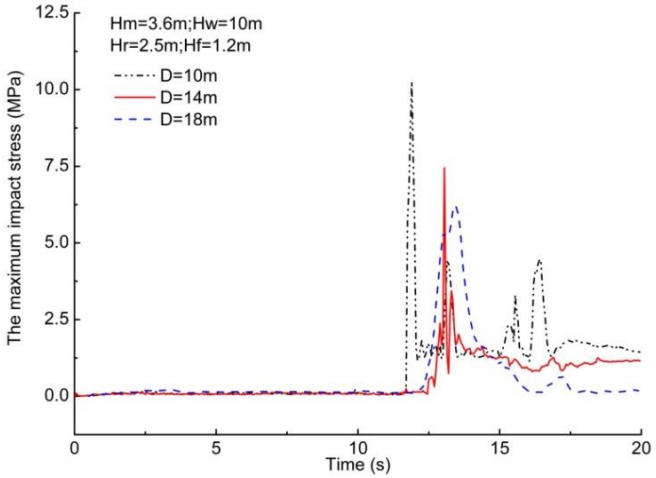

Fig. 14 Stress response of rear wall structure

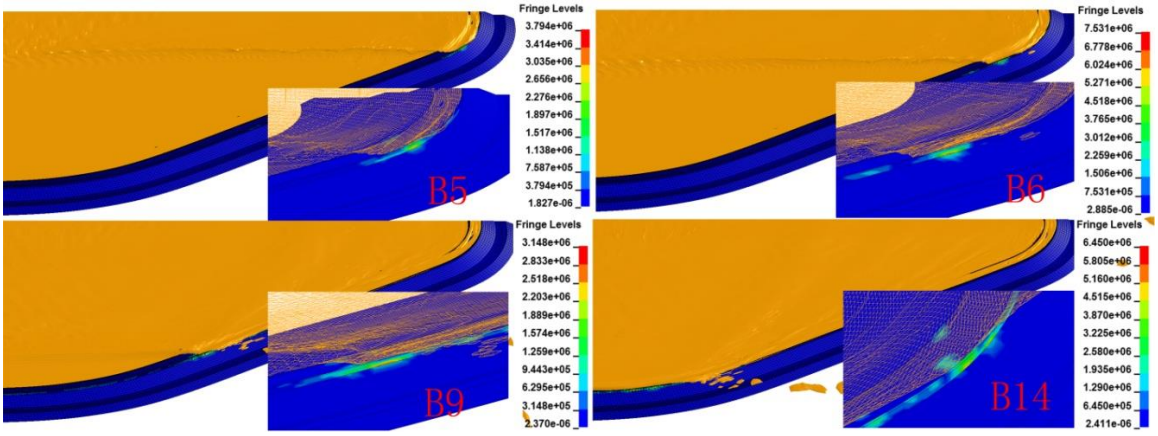

Fig. 15 Snapshots of wave-breakwater interactions

The maximum pressure impulses on the rear seawall for various breakwater widths are plotted in Fig. 13(d). The plot shows that increasing the breakwater width by 4 m based on the design width, decreases the maximum impact pressure on the rear wall by approximately ten percent. However, if the breakwater width decreases by 4 m based on the design width, the maximum impact pressure on the rear wall increases by approximately sixty-four percent.

Fig. 14 shows the maximum stress curves of the breakwater structure for different breakwater widths. The graph shows that the maximum stress for the structures is reached at different times. The figure clearly shows that the structures quiver from the impact of the fluid, and the stress of the structure decreases when the breakwater width increases.

5.3 Application to large-scale breakwaters

Fig. 15 shows three-dimensional snapshots of the wave-breakwater interactions. The figure clearly shows the generation of a solitary wave and that the position of the maximum stress moves

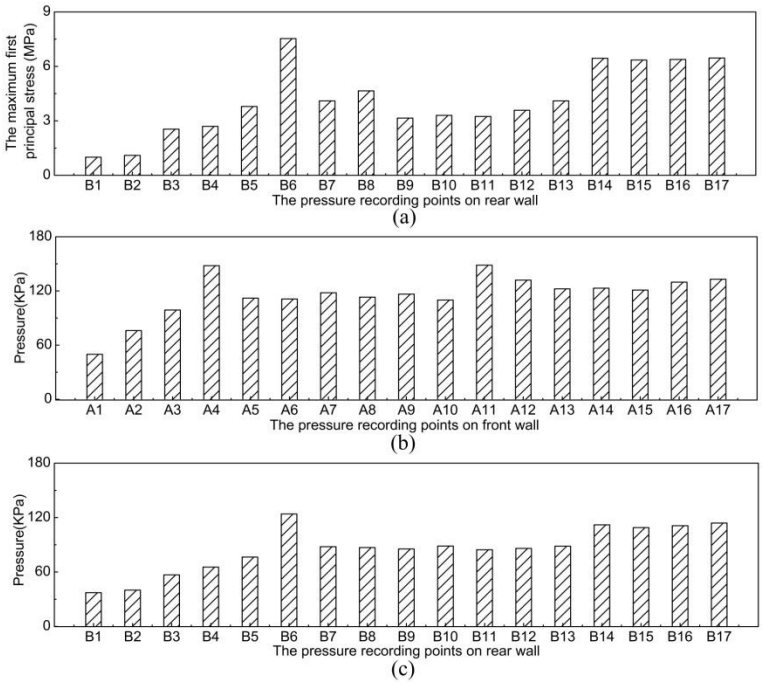

Fig. 16 Maximum wave pressure and structural stress

along with the propagating wave. The maximum impact stress is located at the bottom of the rear wall, and its horizontal distribution is shown in Fig. 16(a).

The horizontal distributions of the maximum wave pressure on the seawalls are shown in Figs. 16 (b) and (c). In Fig. 16(b), two peaks appear on the pressure curve of the front wall at A4 and A11. The peaks are located just at the junctions of the curved and straight segments where the structure axis directions change suddenly. In the computational results, a peak in the pressure curve of the rear wall appears at B6, as shown in Fig. 16(c). The wave overtopping and wave flow along the breakwater axial direction upon the breakwater top cause the wave pressures to undergo a sharp drop after the first curved segment. Finally, the wave impacts the breakwater vertically. The wave pressure at the recorded points (B14-B17) increases monotonically to 120 KPa and remains constant at this level.

6. Conclusions

The ALE method is applied to numerically simulate the interaction between waves and elastic breakwaters. In this method, the fluid and structure are described using a multi-material ALE scheme and a Lagrangian scheme, respectively. The ALE method is combined with an explicit integration scheme, and the Newtonian fluid is assumed to be weakly compressible. The penalty method is used to investigate the interaction between the fluid and the breakwater and the dynamic contact between the structures.

A numerical breakwater-flume coupling model, which replicates the physical model, and a large-scale breakwater - wave coupling model are developed in Hypermesh. The propagation of the

solitary wave and its interaction with the breakwater are reproduced using LS-DYNA MPP on the Dawning supercomputer. The numerical approaches and the model are validated using experimental and theoretical data. The following conclusions are drawn from this study.

• The approaches and models employed in this paper provide an effective way of predicting the wave pressure and the dynamic responses of the breakwater.

• A local breakwater - wave coupling FE model is used to determine the vertical distribution of the maximum wave pressure on both the front and rear seawalls. The structural response effect increases the spill-way impact load of the fluid on the front seawall. In contrast, the structural response decreases the pressure from the violent impact at the rear seawall.

• The effects of the seawall elevation and breakwater width are studied. The front seawall and the embankment top protect the rear seawall. Especially when the breakwater width decreases, the wave pressure and the structural stress of the rear wall are increased significantly. Additionally, on the premise of the wave overtopping satisfaying the design requirements, the elevation of rear seawall should be as low as possible.

• The horizontal distributions of the wave pressures and the structural stress exhibit two primary peaks at the curved segments. The maximum pressure appears at the junctions of the curved and straight segments similarly to the breakwater stress. The numerical simulation shows that the position of the maximum stress moves along with the propagating wave.

Acknowledgements

This work is supported by the National 863 Program (No. 2012AA01A307) and the National Natural Science Foundation of China (No. 51475287; No. 11272214). We gratefully acknowledge the State Key Laboratory Mechanical System and Vibration (Shanghai Jiao Tong University), the Shanghai Nuclear Engineering Research and Design Institute, and the Shanghai Supercomputer Center.

Reference

Anghileri, M., Castelletti, L.M.L. and Tirelli, M. (2005), "Fluid-structure interaction of water filled tanks during the impact with the ground", *Int. J. Impact Eng.*, **31**(3), 235-254.

Antoci, C., Gallati, M. and Sibilla, S. (2007), "Numerical simulation of fluid-structure interaction by SPH", *Comput. Struct.*, **85**(11-14), 879-890.

Bathe, K.J., Zhang, H. and Ji, S. (1999), "Finite element analysis of fluid flows coupled with structural interactions", *Comput. Struct.*, **72**, 1-16.

Cuomo, G., Allsop, W., Bruce, T. and Pearson, J. (2010), "Breaking wave loads at vertical seawalls and breakwaters", *Coast. Eng.*, **57**(4), 424-439.

Guanche, R., Losada, I.J. and Lara, J.L. (2009), "Numerical analysis of wave loads for coastal structure stability", *Coast. Eng.*, **56**(5-6), 543-558.

Hirt, C.W., Amsden A.A. and Cook J.L. (1997), "An arbitrary lagrangian eulerian computing method for all flow speeds", *J. Comput. Phys.*, **135**(2), 203-216.

Hsiao, S. and Lin, T. (2010), "Tsunami-like solitary waves impinging and overtopping an impermeable seawall: experiment and RANS modeling", *Coast. Eng.*, **57**(1), 1-18.

Hajivalie, F. and Yeganeh-Bakhtiary, A. (2011), "Numerical simulation of the interaction of a broken wave and a vertical breakwater", *Int. J. Civil Eng.*, **9**(1), 71-79.

Kalro, V. and Tezduyar, T.E. (2000), "A parallel 3D computational method for fluid-structure interactions in parachute systems", *Comput. Meth. Appl. Mech. Eng.*, **190**(3-4), 321-332.
Losada, I.J., Lara, J.L., Guanche, R. and Gonzalez-Ondina, J.M. (2008), "Numerical analysis of wave overtopping of rubble mound breakwaters", *Coast. Eng.*, **55**(1), 47-62.
Nitikitpaiboon, C. and Bathe, K.J. (1993), "An arbitrary lagrangian-eulerian velocity potential formulation for fluid-structure interaction", *Comput. Struct.*, **47**(4-5), 871-891.
Pal, N.C., Bhattacharyya, S.K. and Sinha, P. K. (2003), "Non-linear coupled slosh dynamics of liquid-filled laminated composite container: a two dimensional finite element approach", *J. Sound Vib.*, **261**(4), 729-749.
Paik, S.H., Moon, J.J., Kim S.J. and Lee, M. (2006), "Parallel performance of large scale impact simulations on linux cluster super computer", *Comput. Struct.*, **84**(10-11), 732-741.
Pin, F.D., Idelsohn, S., Onate, E. and Aubry, R. (2007), "The ALE/Lagrangian Particle Finite Element Method: A new approach to computation of free-surface flows and fluid–object interactions", *Comput. Fluid.*, **36**, 27-38.
Rafiee, A. and Thiagarajan, K.P. (2009), "An SPH projection method for simulating fluid-hypoelastic structure interaction", *Comput. Meth. Appl. Mech. Eng.*, **198** (33-36), 2785-2795.
Souli, M., Ouahsine, A. and Lewin, L. (2000), "ALE formulation for fluid-structure interaction problems", *Comput. Meth. Appl. Mech. Eng.*, **190**(5-7), 659-675.
Sakakiyama, T. and Liu, P. (2001), "Laboratory experiments for wave motions and turbulence flows in front of a breakwater", *Coast. Eng.*, **44**, 117-139.
Sriram, V. and Ma, Q.W. (2012), "Improved MLPG_R method for simulating 2D interaction between violent waves and elastic structures", *J. Comput. Phys.*, **231**(22), 7650-7670.
Tallec, P.L. and Mouro, J. (2000), "Fluid structure interaction with large structural displacements", *Comput. Meth. Appl. Mech. Eng.*, **190** (24-25), 3039-3067.
Yang, C., Lu, H.D. and Löhner, R. (2010), "On the simulation of highly nonlinear wave-breakwater interactions", *Proc. of 9th International Conference on Hydrodynamics*, Shanghai, China, October.
Zhu, F., Zhu, W.H., Fan, J., Fang, B. and Zhao, K. (2012), "Modeling and Analysis of Numerical Wave Tank Based on the ALE Algorithm", *Proc. of 2012 International Conference on Modeling, Identification and control*, Wuhan, China, June.
Zhao, X. and Hu, C. (2012), "Numerical and experimental study on a 2-D floating body under extreme wave conditions", *Appl. Ocean Res.*, **35**, 1-13.